

Transfer learning for affordable and high quality tunneling splittings from instanton calculations

Silvan Käser,[†] Jeremy O. Richardson,[‡] and Markus Meuwly^{*,†}

[†]*Department of Chemistry, University of Basel, Klingelbergstrasse 80, CH-4056 Basel, Switzerland*

[‡]*Laboratory of Physical Chemistry, ETH Zurich, 8093 Zurich, Switzerland*

E-mail: m.meuwly@unibas.ch

August 3, 2022

Abstract

The combination of transfer learning (TL) a low level potential energy surface (PES) to a higher level of electronic structure theory together with ring-polymer instanton (RPI) theory is explored and applied to malonaldehyde. The RPI approach provides a semiclassical approximation of the tunneling splitting and depends sensitively on the accuracy of the PES. With second order Møller-Plesset perturbation theory (MP2) as the low-level (LL) model and energies and forces from coupled cluster singles, doubles and perturbative triples (CCSD(T)) as the high-level (HL) model, it is demonstrated that CCSD(T) information from only 25 to 50 judiciously selected structures along and around the instanton path suffice to reach HL-accuracy for the tunneling splitting. In addition, the global quality of the HL-PES is demonstrated through a mean average error of 0.3 kcal/mol for energies up to 40 kcal/mol above the minimum energy structure (a factor of 2 higher than the energies employed during TL) and $< 2 \text{ cm}^{-1}$ for harmonic frequencies compared with computationally challenging normal mode calculations at the CCSD(T) level.

1 Introduction

Tunneling splittings are exquisitely sensitive to the accuracy of a molecular potential energy surface (PES). The nuclear wave-functions corresponding to the two or multiple quantum mechanical bound states involved in the split energy levels probe an extended region on the underlying PES. Furthermore, the tunneling splitting also informs about the barrier height and the shape of the PES in the region connecting the two wells, see Figure 1. Due to all the above, tunneling splittings constitute a meaningful and stringent test of the level of theory at which the underlying PESs were calculated and the accuracy of their representation required for simulations from which the splittings are determined.

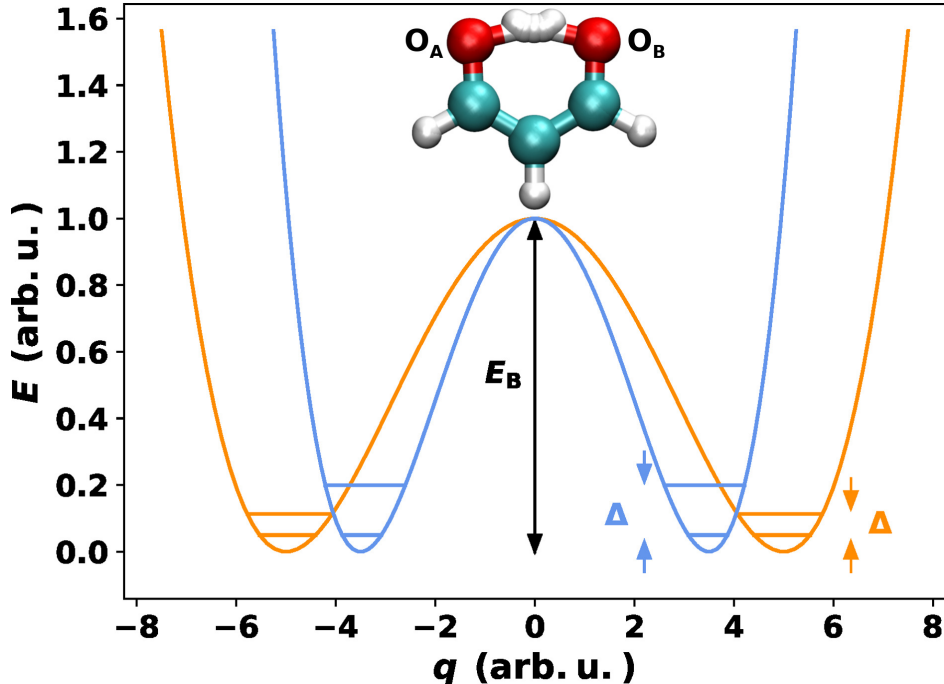


Figure 1: Schematic illustration of two symmetric double-well potentials with the same energy barrier E_B but differing curvatures and tunneling splittings Δ . Malonaldehyde and its instanton path are shown.

Even if a PES is given, accurate computation of tunneling splittings for multidimensional systems from quantum-based methods itself is a formidable task. The ring-polymer instanton (RPI) approach provides a semiclassical approximation of a tunneling process and can be used to calculate tunneling splittings in molecular systems.¹⁻⁴ As was shown for the formic acid dimer,⁴ it is necessary to include all degrees of freedom of the molecule for a quantitative comparison with experiment. This often means that the (semiclassical) full-dimensional instanton approximation is more accurate than a reduced-dimensional quantum calculation. Instanton theory is based on the path-integral formulation of quantum mechanics and is formally exact only in the limit of $\hbar \rightarrow 0$.⁵ In many previous studies it has been shown to give predictions within about 20% of fully quantum-mechanical calculations using the same PES for typical molecular systems, as long as the barrier height is significantly higher than the zero-point energy along the tunneling mode.^{1,4,6} Instanton calculations which, contrary to exact quantum calculations such as wave-function propagation,^{7,8} scale well with system

size, are often used in combination with analytical, full-dimensional PESs. Path-integral molecular dynamics (PIMD) simulations also scale well with system size but are considerably more expensive than an instanton calculation.^{9,10}

In principle it is possible to implement the instanton approach using *on-the-fly ab-initio* electronic structure calculations.^{11,12} However, because energies, gradients and Hessians are needed for each ring-polymer bead, this may be impractical for medium-sized molecules if high accuracy from coupled cluster with perturbative triples (CCSD(T)) level of theory is sought. More recent work has been devoted to combining machine learning (ML) and instanton theory to reduce overall computational expense. Gaussian process regression (GPR) has been used to obtain a local fit of the PES around the dominant tunneling pathway to calculate rate constants.¹³ It has been shown that the GPR rate constants are on par with the *ab initio* results, however, reducing the number of required electronic structure calculations by an order of magnitude. Similarly, instanton rate theory has been combined with NNs to obtain the PES more efficiently as compared to the *on-the-fly* approach.^{14,15}

As an alternative, full-dimensional PESs can now be constructed for medium-sized molecules from which tunneling splittings can also be determined using the instanton approach. The generation of ML PESs based on large data sets of *ab initio* data is a challenging task¹⁶ and accuracy as well as the level of theory of the PES is of crucial importance for the accurate determination of tunneling splittings. The “gold standard” CCSD(T) approach scales as N^7 (with N being the number of basis functions)¹⁷ which quickly becomes computationally prohibitive for generating data to build a full-dimensional PESs even for relatively small molecules. To avoid the need for calculating large *ab initio* data sets at high levels of theory transfer learning (TL)¹⁸⁻²⁰ and related Δ -ML²¹ were shown to be data and cost-effective alternatives.²²⁻²⁷

The combination of TL and instanton theory appears particularly appealing as the instanton path (IP) can be determined on a low-level PES, which gives a rough approximation to the true tunneling path, and can be included (and iteratively refined if needed) into the TL data set. Additionally, the IP is inherently local and, thus, allows concentrating on improving only a small part of a PES. While instanton theory has been used in combination with ML schemes,^{13,15,28} the present work demonstrates the first combination of instanton theory with TL. The capability of the combined approach is demonstrated for the extensively studied malonaldehyde system exhibiting intramolecular hydrogen transfer (HT).

Ring Polymer Instanton theory has been employed to calculate the tunneling splitting of malonaldehyde on a permutationally invariant polynomial (PIP) PES fitted to 11147 near basis-set-limit frozen-core CCSD(T) electronic energies.²⁹ The splitting was found to be 25 cm⁻¹ with RPI⁶ as well as with a strongly related instanton method.³⁰ The same PES was also used to calculate tunneling splittings using the *fixed-node* diffusion Monte Carlo (DMC) method giving 21.6 cm⁻¹ with a statistical uncertainty of 2 to 3 cm⁻¹.²⁹ For DT, computed values on the PIP PES are 3.3 and 3.4 cm⁻¹ using RPI⁶ and the related instanton method,³⁰ and $3.0 \pm 2 - 3$ cm⁻¹ from DMC simulations.²⁹ The tunneling splitting from RPI calculations on a LASSO fit to CCSD(T)(F12*) energies was found to be 19.3 cm⁻¹.^{6,31} To validate such computations, direct comparison with experiment is also of interest. Reliable tunneling splittings from experiment are only available for a few select systems.³²⁻³⁹ For malonaldehyde, the experimentally determined tunneling splitting is 21.583 cm⁻¹ and 2.915 cm⁻¹ for HT and deuterium transfer (DT), respectively.^{32,33,40} Although these results are not in perfect agreement with experiment, they are close enough that spectroscopic assignments can be made and provide detailed mechanistic information about the tunneling process.

The purpose of the present work is to develop and quantitatively assess an evidence-based

procedure to determine reliable tunneling splittings by combining transfer learned PESs with instanton calculations. It is shown that this can dramatically reduce the cost of the overall simulation in comparison to working with *ab initio* potentials. The work is structured as follows. First, the methods and the generation of the data sets are presented. This is followed by a thorough evaluation of the accuracy of the transfer learned PESs in terms of tunneling splittings and harmonic frequencies. Finally, the results are discussed and conclusions are drawn.

2 Methods

2.1 Ring-Polymer Instanton Theory

In a one-dimensional model, instanton theory is strongly related to the WKB approximation.⁴¹ Its main advantage, however, is that it can also be applied to multidimensional systems, in which it locates the uniquely defined optimal tunneling pathway.⁴² This pathway, known as the instanton, is defined as a long imaginary-time $\tau \rightarrow \infty$ path connecting two degenerate wells which minimizes the action, S . In computations, the path is located using an efficient ring-polymer optimization based on discretizing the path into N ring-polymer beads and taking the limit $N \rightarrow \infty$ (typically on the order of 1000 is sufficient for convergence). The action is determined by the distance between neighbouring beads as well as the potential-energy of each bead, i.e. it uses information *along* the IP. Full technical details are presented in previous work.^{1,2} In general, the IP is not equivalent to the minimum-energy pathway (MEP) and will not even pass through a saddle point. This is because the instanton finds a compromise between length and height to optimize the tunneling path. Unlike PIMD or DMC, no random numbers or statistical errors are involved and so the instanton (once it is converged with $\tau \rightarrow \infty$ and $N/\tau \rightarrow \infty$) is in principle uniquely determined by the PES.

Once the IP has been located, fluctuations around the path are computed to second order and the information is combined into the term Φ , i.e. this is based on information *around* the IP. For this, one requires the Hessians (second-derivative matrix of PES) at each bead. The final prediction for the tunneling splitting (in a double-well system) is given by

$$\Delta = \frac{2\hbar}{\Phi} \sqrt{\frac{S}{2\pi\hbar}} e^{-S/\hbar}. \quad (1)$$

Because S appears in the exponent it is particularly important to determine this quantity with high accuracy.

The method has also been generalized to treat tunneling in systems with multiple (more than two) wells^{3,43} and in cases with non-degenerate wells for instance due to asymmetric isotopic substitution.⁶ The approach outlined in this work is, in principle, also applicable to these extensions.

2.2 Machine Learning

All PESs used in this work are represented with a high-dimensional neural network (NN) of the PhysNet⁴⁴ architecture. PhysNet is a ‘message-passing’⁴⁵ NN that employs learnable descriptors of the atomic environments to predict individual atomic energy contributions E_i and partial charges q_i . The descriptors are initialized as $\mathbf{x}_i^0 = \mathbf{e}_{Z_i}$, where \mathbf{e}_{Z_i} corresponds to a parameter vector defined by the nuclear charge Z_i , i.e. atoms of the same element share the same descriptor. The descriptor is then iteratively updated and refined to best describe the local chemical environment of each atom i by passing ‘messages’ between atoms within a cut-off r_{cut} following

$$\mathbf{x}_i^{l+1} = \mathbf{x}_i^l + \sum_{r_{ij} < r_{\text{cut}}} \mathcal{F}(\mathbf{x}_i^l, \mathbf{x}_j^l, r_{ij}). \quad (2)$$

where r_{cut} was 10 Å. Here, \mathbf{x}_i^l and \mathbf{x}_j^l are the descriptors of atoms i and j at iteration l , r_{ij} is their interatomic distance and $\mathcal{F}(\mathbf{x}_i^l, \mathbf{x}_j^l, r_{ij})$ is the ‘message-passing’ function (for details see Ref. 44). Because only pairwise distances are used to encode the atoms’ chemical environment and summation is commutative, the resulting descriptors (and thus the PES) are invariant with respect to translation, rotation and permutation of identical atoms, which is of particular importance when describing tunneling between degenerate wells. The descriptors are then used to predict partial charges q_i (which are corrected to ensure total charge conservation) and the total energy of the chemical system by summation of the atomic contributions and explicitly including long-range electrostatics according to

$$E = \sum_i E_i + k_e \sum_{i=1}^N \sum_{j>i}^N \frac{q_i q_j}{r_{ij}} \quad (3)$$

Here, k_e represents Coulomb’s constant and the second term involving $\frac{q_i q_j}{r_{ij}}$ is damped to avoid numerical instabilities caused by the singularity at $r_{ij} = 0$ (for details refer to Ref. 44). The forces \mathbf{F} and Hessians \mathbf{H} can be obtained analytically using reverse mode automatic differentiation⁴⁶ as implemented in Tensorflow.⁴⁷

The learnable parameters of PhysNet are fitted to reference *ab initio* energies, forces and dipole moments following the strategy outlined in Reference 44. The partial charges q_i are fitted to the *ab initio* dipole moment ($\mu = \sum_i^N q_i \mathbf{r}_i$) and explicitly enter the energy expression (see equation 3). In the present work, the TL scheme is employed whereby the parameters of a low-level (LL) treatment are used as a meaningful initial guess and are fine-tuned using higher-level information. For TL, the learning rate is reduced from 10^{-3} (as for learning a model from scratch) to 10^{-4} . The LL in the present work is the full-dimensional PES for malonaldehyde at the MP2/aug-cc-pVTZ level of theory (henceforth, PhysNet MP2 PES) which is available from previous work and was trained on ~ 70000 reference structures.²² This PhysNet PES has a barrier for HT of 2.79 kcal/mol which compares to a reference value

of 2.74 kcal/mol calculated at the MP2/aug-cc-pVTZ level of theory and the reference harmonic frequencies are reproduced with a root-mean-square deviation (RMSD) of 3.6 cm^{-1} . The high-level (HL) treatment is the considerably higher and computationally much more demanding CCSD(T)/aug-cc-pVTZ level of theory at which energies, forces and dipole moments are calculated using Molpro⁴⁸ for all data points used in TL.

2.3 Data Set Generation

Transfer learning requires high-level energies, forces and dipole moments for selected geometries of the system considered and ideally cover all spatial regions relevant for the observable(s) of interest. Without additional *a priori* information it is advantageous to generate an initial pool of structures which can be used for TL to fine-tune the LL treatment. When selecting configurations, it is not necessary to sample both potential wells since PhysNet handles this symmetry by construction. Here, the initial pool contained 862 malonaldehyde configurations consisting of:

- 111 geometries along the MEP of the PhysNet MP2 PES.
- 110 geometries along the IP of the PhysNet MP2 PES.
- 111 geometries along the IP determined on a PES that was transfer learned by using CCSD(T) information of the 111 MEP geometries (see above) to have an energy barrier closer to the *ab initio* CCSD(T) barrier.
- 280 geometries obtained from normal mode sampling (NMS) around the equilibrium geometry. For this purpose, normal mode vectors and corresponding force constants are determined *ab initio* at the MP2/aug-cc-pVTZ level of theory.
- 240 geometries around the IP as obtained from NMS.
- 10 geometries along the IP of TL₁ (see Section 3.2).

This data set is referred to as the ‘‘Extended Data Set’’ and transfer learned models using it are called TL_{ext} . To probe the dependence of barrier heights and tunneling splittings on details of the training, ten independent models were trained on different splits of the data for TL_{ext} (and all the subsequent TMs). For each of the ten resulting PESs an instanton calculation was carried out. From this information, averages and standard deviations for the barrier heights and tunneling splittings were determined.

After validating the performance of TL_{ext} from instanton calculations on each of the independently trained models, smaller subsets of the Extended Data Set were selected, employed for TM and subsequent tunneling splitting calculations.

3 Results

To set the stage, the tunneling splittings for malonaldehyde were calculated on the PhysNet MP2 PES using RPI theory. The tunneling splitting calculations were carried out with three different values of the imaginary time, τ , corresponding to effective ‘temperatures’ $T = \hbar/k_B\tau \in [50, 25, 12.5]$ K and with different numbers of beads $N \in [2^5, \dots, 2^{12}]$ to ensure convergence. Formally the instanton result is defined in the low-temperature limit, which is equivalent to infinitely-long imaginary times. The results are summarized in Table S1. A tunneling splitting of 96 cm^{-1} is obtained compared with 25 cm^{-1} from instanton calculations^{6,30} on the PIP-representation²⁹ of the CCSD(T) reference data and 21.6 cm^{-1} from experiments.^{32,33,40} This illustrates the insufficient quality of the MP2 level of theory to capture tunneling splittings correctly. For the following, all instanton calculations were carried out with $N = 4096$ beads at an effective temperature of $T = 25$ K, which was found to be more than sufficient for convergence of Δ to two significant figures.

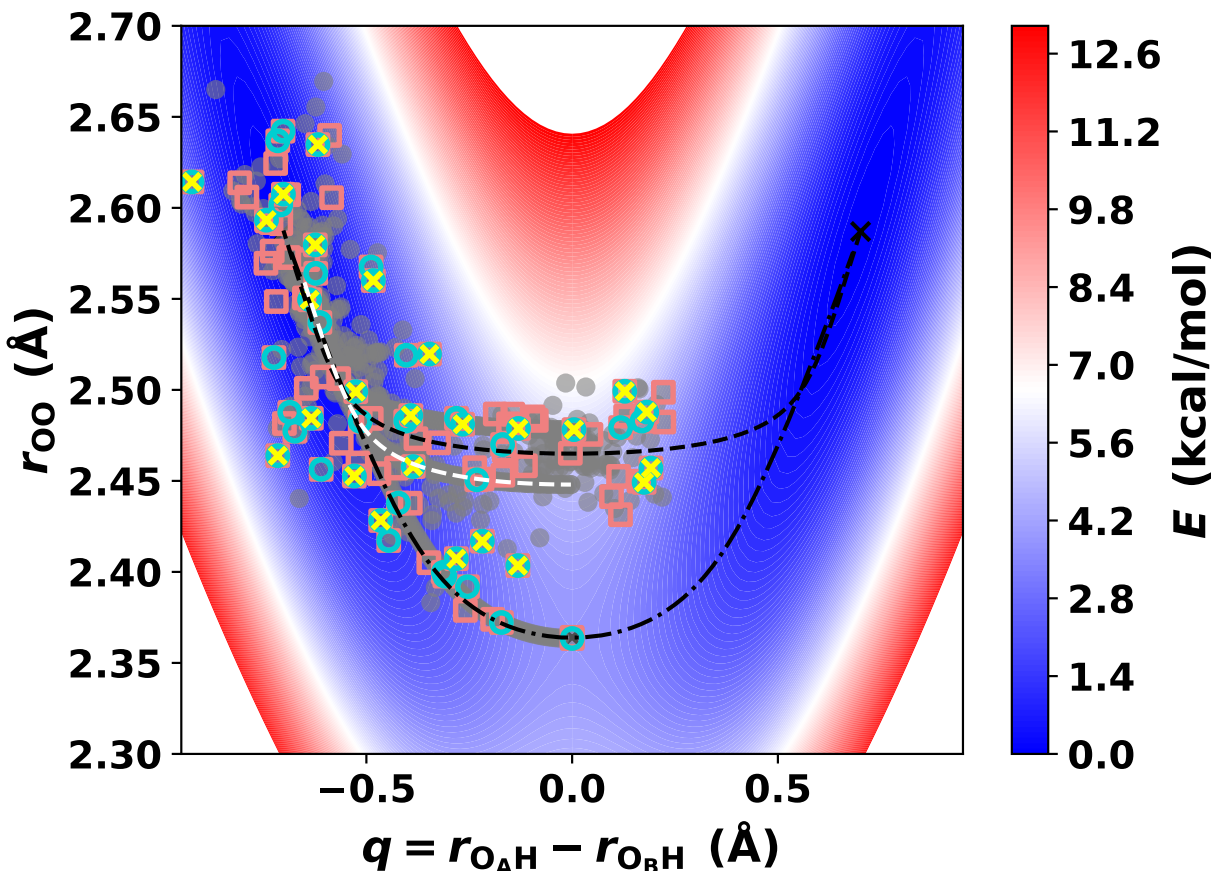


Figure 2: Data sets used for TL projected onto a 2D cut through the TL_{ext} PES spanned by the O–O distance and the reaction coordinate $q = r_{\text{OAH}} - r_{\text{OBH}}$, for labels see Fig. 1. The Extended Data Set (862 structures, gray circles) is shown together with sets for TL_0 (25 structures, yellow crosses), TL_1 (50 structures, turquoise circles), and TL_2 (100 structures, salmon squares). The MEP and the instanton path (as determined on the TL_{ext} PES) are marked with a dash-dotted and a dashed line, respectively. The IP on the PhysNet MP2 PES is the white dashed line and clearly differs from that (black dashed) on the CCSD(T) PES.

3.1 Performance of TL_{ext}

As a reference for the following exploration, the performance of TL_{ext} using the full set of 862 energies, forces and dipole moments determined at the CCSD(T)/aug-cc-pVTZ level is first assessed. These geometries are shown as a projection onto the PES spanned by the O–O distance and the reaction coordinate $q = r_{\text{OAH}} - r_{\text{OBH}}$ in Figure 2 (gray circles). As the PES is symmetric with respect to $q = 0$, the same geometry appears to the left and to the right of the mirror plane. The Extended Data Set was split according to $\sim 80/10/10\%$

into training/validation/test sets, from which the test sets were used only for testing. Across the 10 TL models, the separate test sets were predicted on average with $\text{MAE}(E) \approx 0.006$, $\text{RMSE}(E) \approx 0.009$ kcal/mol, $\text{MAE}(F) \approx 0.03$ and $\text{RMSE}(F) \approx 0.07$ kcal/mol/Å. The average barrier height on the ten transfer-learned PESs ($\langle \text{TL}_{\text{ext}} \rangle$) was $E_B = 3.8945 \pm 0.0006$ kcal/mol which compares with an *ab initio* barrier of 3.8948 kcal/mol determined at the CCSD(T)/aug-cc-pVTZ level of theory determined from present calculations. The RPI tunneling splittings for HT and DT were $\Delta_H = 25.3 \pm 0.2$ cm⁻¹ and $\Delta_D = 3.7 \pm 0.03$ cm⁻¹, respectively, see Table 1 and S2. These results compare with computed splittings on the PIP representation of CCSD(T)/aug-cc-pVTZ reference calculations using instanton calculations that yield 25/3.4 cm⁻¹^{16,30} and experimental splittings of 21.6/2.9 cm⁻¹.^{32,33,40} Hence, the transfer-learned PES using fewer than 1000 higher level CCSD(T)/aug-cc-pVTZ energies and forces together with the same method for determining the tunneling splitting performs on par with calculations on the PIP representation of the ~ 11000 CCSD(T)/aug-cc-pVTZ energies.²⁹ Based on this it is of much practical interest to further reduce the number of HL calculations required to achieve the same result. Therefore, in a next step, different subsets of the Extended Data Set are considered and used for TL to arrive at an ideally small number of HL points while still retaining the accuracy in tunneling splittings from instanton calculations.

Table 1: Energy barriers E_B (kcal/mol), tunneling splittings Δ (in cm⁻¹) at $T = 25$ K and with $N = 4096$, action S/\hbar and fluctuation factor Φ (in a.u. of time \hbar/E_h) for malonaldehyde determined from TL_{ext} and $\text{TL}_{0,1,2}$ PESs. The *ab initio* barrier height for HT at the CCSD(T)/aug-cc-pVTZ level of theory is 3.8948 kcal/mol.

	N_{data}	E_B	Δ_H	S/\hbar	Φ
MP2	70k	2.7889	96.3	4.502	42.770
$\langle \text{TL}_0 \rangle$	25	3.8925 ± 0.0119	23.4 ± 1.9	5.749 ± 0.026	57.405 ± 4.486
$\langle \text{TL}_1 \rangle$	50	3.8974 ± 0.0161	24.9 ± 1.1	5.764 ± 0.012	53.096 ± 2.375
$\langle \text{TL}_2 \rangle$	100	3.8941 ± 0.0021	25.2 ± 0.5	5.748 ± 0.005	53.053 ± 1.156
$\langle \text{TL}_{\text{ext}} \rangle$	862	3.8945 ± 0.0006	25.3 ± 0.2	5.743 ± 0.002	53.241 ± 0.454

3.2 Performance on Smaller Datasets: TL_0 , TL_1 , and TL_2

From the Extended Data Set containing 862 geometries, different subsets were extracted. The size of the data set has to be chosen small enough for efficient computation but sufficiently large to still cover the appropriate regions of configurational space probed by the instanton calculation.

TL_0 : To check whether a considerably smaller data set suffices as a starting point, ten TIs were performed on a data set containing only 25 geometries: a) 5 IP geometries (approximately equally spaced) determined on a PES that was transfer learned to have a barrier closer to the *ab initio* CCSD(T) barrier; b) 10 geometries, each, selected from the NMS around the equilibrium geometry and the IP. This can be done by selecting geometries based on a RMSD criterion on the n atomic positions ($\sqrt{\frac{1}{n} \sum_{i=1}^n \|v_i - w_i\|^2}$ where v_i and w_i are two sets of Cartesian coordinates of atom n), which was done as follows for both groups of geometries that were generated with NMS. Starting from a random geometry, new geometries are added iteratively if the RMSD with respect to the selected ones is larger than a threshold. For this reason, the threshold is maximized to include 10 geometries. Note that no MEP geometries are added. The data set for TL_0 are the yellow crosses in Figure 2.

With this smallest subset the barrier height of the (ensemble of the) transfer learned PES $\langle \text{TL}_0 \rangle$ is $E_B = 3.8925 \pm 0.012$ kcal/mol which is, within errors, close to the target value of 3.8948 kcal/mol determined at the CCSD(T)/aug-cc-pVTZ level. From 10 independent instanton calculations the average splitting is $\Delta_H = 23.4 \pm 1.9$ cm^{-1} which is ~ 2 cm^{-1} below that from the simulations on the TL_{ext} PES but still within statistical fluctuation. Comparing the action S/\hbar of the IPs on TL_0 and TL_{ext} shows that they are comparable (5.743 ± 0.002 vs. 5.749 ± 0.026) and even identical within the error bars. However, the uncertainty on TL_0 is larger by an order of magnitude compared with that on TL_{ext} . Thus, the action, S/\hbar , of the path is clearly less well defined on TL_0 . For the fluctuation factor

Φ the differences are considerably larger between the two families of PESs. Still, the values themselves are within error bounds but again, the fluctuation around the mean for TL_0 is ten times larger than that for the TL_{ext} PESs. This conclusion also holds for DT, see Table S2. Overall, using only 25 additional data points as done for TL_0 already yields encouraging results for the barrier height and tunneling splittings. To explore further improvements new points were added and the process was repeated.

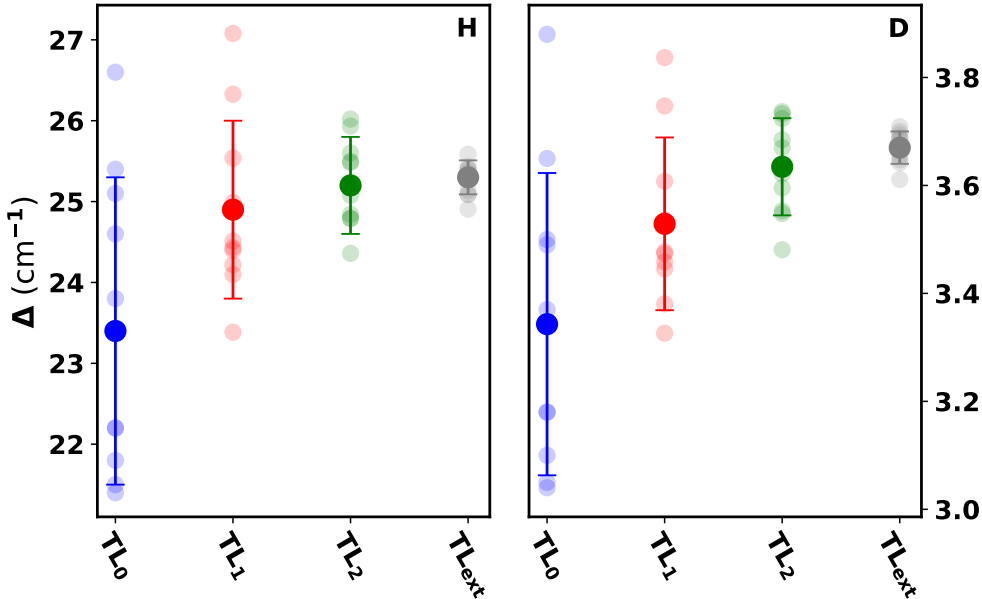


Figure 3: Tunneling splittings for H- and D-transfer (left and right panels) from all TL PESs (transparent circles). The corresponding averages (opaque circle) and standard deviations (error bars as $\pm\sigma$) as obtained from TL_0 (blue), TL_1 (red), TL_2 (green) and TL_{ext} are reported, too. Comprehensive lists of the tunneling splittings for all TL PESs are given in Tables S3 to S6.

TL_1 : For TL_1 the points used for TL_0 were extended and increased to 50 points, see turquoise circles in Figure 2. The data set for TL_1 contained: a) 5 geometries along the MEP of the PhysNet MP2 PES; b) 5 geometries along the IP of a transfer learned PES from using the MEP points calculated at CCSD(T); c) 20 geometries, each, selected from the NMS around the equilibrium geometry and the IP. The MEP and IP geometries are chosen with a uniform spacing along the respective path and the geometries from NMS are selected following the

RMSD approach outlined for TL_0 .

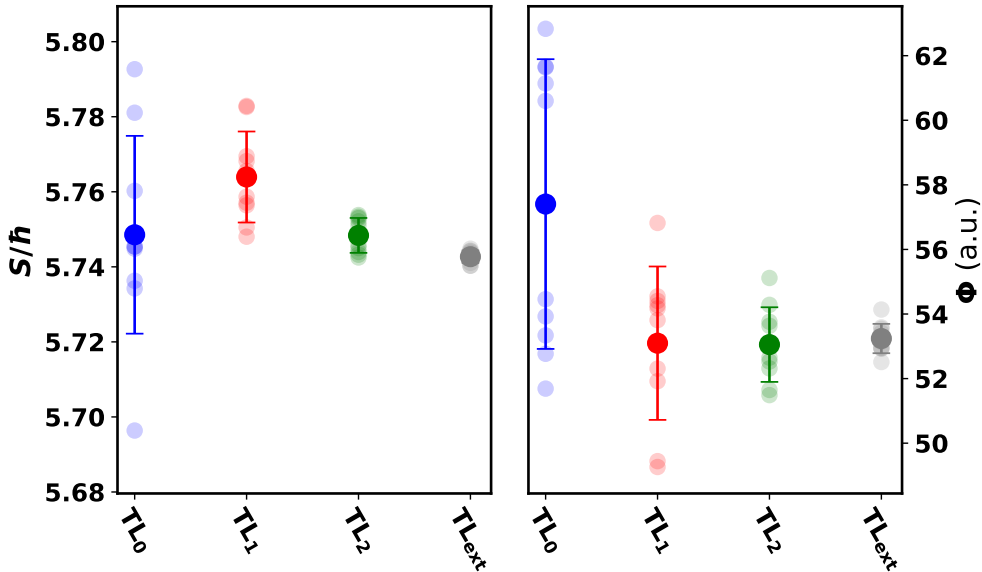


Figure 4: Action S/\hbar (left panel) and fluctuation factor Φ (right panel) from all TL PESs (transparent circles) for HT (for DT see Figure S5). The corresponding averages (opaque circle) and standard deviations (error bars as $\pm\sigma$) as obtained from TL_0 (blue), TL_1 (red), TL_2 (green) and TL_{ext} are indicated as well.

TL_1 yields an averaged barrier height $E_B = 3.8974 \pm 0.0161$ which agrees within error bars with that of TL_{ext} and the *ab initio* value (3.8948 kcal/mol). The splitting $\Delta_H = 24.9 \pm 1.1$ cm^{-1} is only 0.4 cm^{-1} below that of TL_{ext} . The key improvement is that the fluctuation factor Φ agrees considerably better with TL_{ext} than for TL_0 and the remaining 2% discrepancy can be traced to the 0.02 absolute difference in S/\hbar . Overall, increasing the number of geometries used for TL to $N_{data} = 50$ in this fashion leads to a PES which reproduces the barrier height and splittings from TL_{ext} . To further probe convergence of these results yet a larger data set was considered.

TL_2 : While the accuracy of TL_1 might appear satisfactory, convergence of TL_1 cannot be checked without TL_{ext} . Thus, TL_1 was further extended to yield TL_2 . This was accomplished from a strategy related to adaptive sampling.⁴⁹ Two independent models from TL_1

were used to predict the energy E of the remaining pool of geometries obtained from NMS. From these geometries, the 40 geometries with the largest deviation (here ~ 0.02 kcal/mol) between the prediction of the two NNs are added to the data set. If a large deviation between the energy predictions of the two models is found, it is likely that no or too little reference data has been included in TL_1 . In addition, 5 geometries along the MEP and instanton of the TL_1 were added such that TL_2 contained a total of 100 geometries (see salmon squares in Figure 2).

With TL_2 the barrier height E_B , splitting Δ , action S/\hbar and fluctuation Φ further improve over those from TL_1 and are closer to the results from TL_{ext} , see Table 1 and S2. Within 1σ all values for HT and DT agree with those from TL_{ext} and with the reference from the literature except for the tunneling splitting for DT. Overall, addition of 50 to 100 additional points from the HL treatment appears to suffice to arrive at a quantitatively correct PES transfer-learned from the LL treatment (MP2/aug-cc-pVTZ). Figure 3 illustrates the gradual convergence for TL_0 to TL_2 towards the results found for TL_{ext} , which is promising. While exceptional agreement regarding the energy barrier E_B (as the “simpler” property) is found for all the TMs the standard deviation of the splittings Δ_H (which is more challenging to obtain) can be reduced from 1.9 cm^{-1} (7.5%) for TL_0 to 0.5 cm^{-1} (2%) for TL_2 . The results from TL_2 are accurate to within 0.1 cm^{-1} for HT and 0.04 cm^{-1} for DT as compared to TL_{ext} . This corresponds to deviations of 0.4% and 1.1%. The IPs themselves are reported in Figures S1 to S4 and show slight deviations between the different TMs on the smallest data set (TL_0), but for TL_1 , TL_2 and TL_{ext} they are hardly distinguishable.

In summary, it has been found that with between 25 and 50 HL energies and forces for judiciously chosen structures the correct barrier height, tunneling splitting, action and fluctuation can be obtained, see Table 1. This is the foundation to further optimize the procedure, ideally based entirely on information available from the LL surface by minimizing the

amount of data required from the HL treatment.

3.3 Towards an Optimized Procedure

For an even more efficient procedure, an approach is sought that is based on information about the LL-PES only. Hence, an attempt is made to further reduce the computational effort by minimizing the number of structures for which HL calculations need to be carried out for an improved PES and tunneling splittings. Therefore, it is explored which elements of the procedure are most important for obtaining high accuracy to cost ratios. For moving towards a more evidence-guided, optimized procedure, TL is carried out from LL-information that is only contained in the MEP and IP as follows: a) only the MEP (TL_{MEP}) using 111 geometries along the MEP of the PhysNet MP2 PES; b) only the IP (TL_{IP}) using 110 geometries along the IP of the PhysNet MP2 PES; and c) a combination of the MEP and the IP (TL_{MI}) including 111 MEP and 110 instanton geometries as obtained from the PhysNet MP2 PES. The HL information for TL consisted again of energies, forces and dipole moment determined at the CCSD(T)/aug-cc-pVTZ level of theory. A total of 5 TMs were performed, each on different splits of the data. The two best NNs (judged from the performance on the validation set) were used for further analysis.

First, it is noted that for TL_{MEP} and TL_{MI} the barrier E_B for HT agrees well with the target value of 3.8948 kcal/mol (*ab initio* CCSD(T)/aug-cc-pVTZ level value) whereas this is not the case for TL_{IP} , as expected, because the instanton path does not pass through the transition state of the MEP (see Table 2). Also, despite starting from MP2 information only, TL to the HL model yields considerably improved tunneling splittings Δ_H for all three models, ranging from 15 to 18 cm^{-1} , compared to those from the PhysNet MP2 PES (96 cm^{-1}).

Considering the action S/\hbar from TL_{MEP} , TL_{IP} and TL_{MI} it is seen that it progressively

Table 2: Energy barriers E_B , tunneling splittings Δ_H (at $T = 25$ K and $N = 4096$), action S/\hbar and fluctuation factor Φ (in a.u. of time \hbar/E_h) for HT determined from TL PESs using MEP points only (TL_{MEP}), instanton points only (TL_{IP}), and a combination of MEP and instanton points (TL_{MI}). TL_x^a and TL_x^b correspond to two NNs that are trained on different splits of the data. Note that the energy barrier for TL_{IP} is inaccurate, as expected, because the IP misses the transition state of the PES. The *ab initio* barrier at the CCSD(T)/aug-cc-pVTZ level of theory is 3.8948 kcal/mol.

	E_B [kcal/mol]	Δ_H [cm^{-1}]	S/\hbar	Φ
TL_{MEP}^a	3.94	15.4	5.887	76.482
TL_{MEP}^b	3.95	14.1	5.912	81.921
TL_{IP}^a	3.49	16.7	5.792	76.975
TL_{IP}^b	3.50	16.9	5.794	75.858
TL_{MI}^a	3.90	18.2	5.768	72.262
TL_{MI}^b	3.90	16.9	5.774	77.374
$\langle \text{TL}_{\text{ext}} \rangle$	3.8945	25.3	5.743	53.241

approaches that from TL_{ext} . For TL_{MEP} the action overshoots the target value from TL_{ext} by ~ 0.15 which leads to an error of ~ 15 % in the splitting because S/\hbar appears in the exponential factor in Eq. 1. Conversely, with a difference of 0.04 compared with TL_{ext} , the error for TL_{MI} due to S/\hbar is only ~ 4 %. The influence of Φ on the difference between TL_{ext} and the three models considered in Table 2 is minor because for all of them Φ is uniformly too large by ~ 40 % compared with that from TL_{ext} .

Table 2 suggests that a *combination* of information from the MEP and the IP used for transfer learning, i.e. TL_{MI} , yields E_B and Δ_H closest to the results from TL_{ext} . However, the tunneling splittings still differ by more than 10 % from the target value obtained on the TL_{ext} PESs. Considering the actions S/\hbar and fluctuations Φ for all the transfer learned PESs in Table 2 it is found that in particular the values of Φ , which are sensitive to fluctuations around the IP, differ considerably from that on TL_{ext} . Hence as a last improvement points *along* the MEP and IP are combined with structures *around* the IP.

For two final, evidence-based TMs (TL_{EB1} and TL_{EB2}), a set of 25 data points was generated

Table 3: Energy barriers E_B (kcal/mol), tunneling splittings Δ_H (in cm^{-1}) at $T = 25$ K and with $N = 4096$, action S/\hbar and fluctuation factor Φ (in a.u. of time \hbar/E_h) for malonaldehyde determined from TL_{EB} . The *ab initio* barrier at the CCSD(T)/aug-cc-pVTZ level of theory is 3.8948 kcal/mol.

	N_{data}	E_B	Δ_H	S/\hbar	Φ
MP2	70k	2.7889	96.3	4.502	42.770
$\langle \text{TL}_0 \rangle$	25	3.8925 ± 0.0119	23.4 ± 1.9	5.749 ± 0.026	57.405 ± 4.486
$\langle \text{TL}_1 \rangle$	50	3.8974 ± 0.0161	24.9 ± 1.1	5.764 ± 0.012	53.096 ± 2.375
$\langle \text{TL}_2 \rangle$	100	3.8941 ± 0.0021	25.2 ± 0.5	5.748 ± 0.005	53.053 ± 1.156
$\langle \text{TL}_{\text{ext}} \rangle$	862	3.8945 ± 0.0006	25.3 ± 0.2	5.743 ± 0.002	53.241 ± 0.454
$\langle \text{TL}_{\text{EB1}} \rangle$	25	3.9025 ± 0.0232	23.7 ± 1.1	5.740 ± 0.013	57.099 ± 3.249
$\langle \text{TL}_{\text{EB2}} \rangle$	25	3.9041 ± 0.0189	23.5 ± 2.1	5.733 ± 0.025	58.241 ± 4.850

as follows. A total of 5 points was selected along the MEP and IP (one close to the minimum and 2 points along the PhysNet MP2 PES MEP and IP each, see black points in Figure 5). These were supplemented by 20 geometries from NMS around the equilibrium structure and the IP that are selected by means of an RMSD criterion. For TL_{EB1} (orange circles in Figure 5), the geometries with largest RMSD are selected (single geometries which occupy the same r_{OO} and q coordinates are eliminated). For TL_{EB2} (green crosses in Figure 5), besides the RMSD criterion, the geometries were selected to cover the *important* configurational space more regularly (as judged by Figure 5).

For both sets of points the corresponding CCSD(T)/aug-cc-pVTZ energies, forces and dipole moments were used for TL, resulting in two sets of transfer learned PESs: TL_{EB1} and TL_{EB2} . For both of them the barrier height (3.90 kcal/mol) is within error bars of TL_{ext} for which it was 3.89 kcal/mol. The action S/\hbar for both EB-models agree with TL_{ext} within error bounds although the fluctuations around the mean is larger by almost an order of magnitude, see Table 3. For the fluctuation Φ the differences compared with TL_{ext} are $\sim 5\%$, commensurate with TL_0 and evidently improved over those using MEP, IP or MI, see Table 2 which do not train on geometries around the path. The tunneling splittings are $\Delta_{\text{H,EB1}} = 23.7 \pm 1.1 \text{ cm}^{-1}$ and $\Delta_{\text{H,EB2}} = 23.5 \pm 2.1 \text{ cm}^{-1}$, both of which are close to/within error bounds of the reference value (25.3 ± 0.2), see Table 3. These results are comparable and slightly better

to those on TL_0 which also was based on only 25 points for TL. However, the training data for $TL_{EB1,EB2}$ are selected based *entirely* on the PhysNet MP2 PES whereas TL_0 made use of HL information in that it employed geometries along the IP of a PES with corrected barrier. Hence, from a computational perspective, the EB models are considerably more cost-effective.

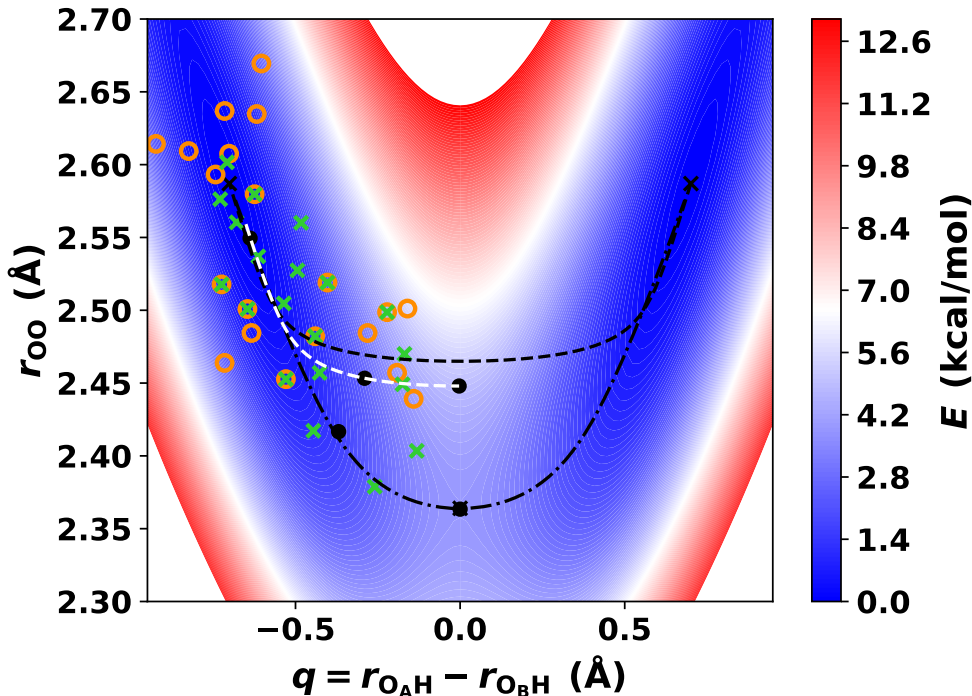


Figure 5: The data sets used for TL_{EB1} (orange circles) and TL_{EB2} (green crosses) are shown on a 2D projection of the PES spanned by the O–O distance and the reaction coordinate $q = r_{O_{AH}} - r_{O_{BH}}$. Both data set contain 25 geometries. The MEP and the IP (as determined on the TL_{ext} PES) are marked with a dash-dotted and a dashed line, respectively. The IP on the MP2 PES is illustrated as white dashed line.

Overall, it is found that TL to the HL with 25 additional points yields a barrier height that agrees with the full HL treatment and the tunneling splitting differs by only $\sim 1 \text{ cm}^{-1}$. Any further improvement requires additional points. Based on the results in Table 3 it is expected that using a TL model trained on fewer than 50 judiciously selected HL data points yields results within 1% of the HL reference TL_{ext} . This needs also be contrasted with an expected

accuracy of instanton calculations for tunneling splittings of $\sim 20\%$.

4 Discussion and Conclusions

The present work aimed at developing a computationally efficient and accurate road-map for how to improve a given LL model - which was assumed to be “comprehensive” (here 7×10^4 MP2 energies and forces were used) for the observable of interest - to a HL model by providing a small amount of additional information at the higher level of theory considering a particular observable. Here, the observable was the tunneling splitting for HT/DT in malonaldehyde for which the LL model (MP2/aug-cc-pVTZ) yielded $\Delta = 96 \text{ cm}^{-1}$, compared with a literature value of $\Delta_{\text{H}} \sim 25 \text{ cm}^{-1}$ from a PIP-represented PES of CCSD(T)/aug-cc-pVTZ reference energies using a range of methods for computing $\Delta_{\text{H/D}}$, see Table S7. Most HL models generated were based on TL using 10s to 100s of HL points and yield $\Delta \sim 25 \text{ cm}^{-1}$ which is a substantial improvement over the LL model and consistent with computations in the literature at the same level of theory but employing computationally much more demanding approaches. The remaining differences between computations and experiments are due to a) shortcomings of the CCSD(T) level of theory compared with a full CI treatment, b) the incompleteness of the basis set, and c) inherent semiclassical approximations of instanton theory (e.g. neglect of coupling to overall molecule rotation and anharmonicity perpendicular to the instanton path).

A typically used shortcut is to optimize the instanton using a LL *ab initio* method, e.g. DFT or MP2, and then compute the CCSD(T) properties along the path to correct the action S/\hbar . Such a hybrid approach was assessed using the PhysNet MP2 PES to optimize the instanton and then calculate the action S/\hbar on the TL_{ext} PES.^{11,12,50,51} The results are summarized in Table 4 and illustrate that although the hybrid approach is, in this case, able to

infer the correct value for S/\hbar , the TL approach additionally improves Φ . Using Equation 1 with the action as determined by the hybrid approach ($S/\hbar = 5.7401$) and the fluctuation factor determined on the PhysNet MP2 PES ($\Phi = 42.7705$) yields $\Delta_{\text{H}} \sim 31.5 \text{ cm}^{-1}$ which overestimates the value of 25.1 cm^{-1} from TL_{ext} . The TL approach is thus able to provide a more accurate prediction of Δ for a similar computational cost.

Table 4: Actions S/\hbar and fluctuation factor Φ as obtained from the MP2 PhysNet PES (MP2), on a representative TL_{ext} PES (TL_{ext}) and a hybrid approach optimizing the IP on the PhysNet MP2 PES and using TL_{ext} to obtain CCSD(T) properties along resulting IP⁶

PES	H			D		
	Δ_{H}	S/\hbar	Φ	Δ_{D}	S/\hbar	Φ
MP2	96.3	4.502	42.771	18.8	5.705	73.964
Hybrid	31.5	5.740	42.771	4.4	7.276	73.964
$\langle \text{TL}_{\text{EB2}} \rangle$	23.5	5.733	58.241	3.5	7.266	94.777
TL_{ext}	25.1	5.744	53.586	3.6	7.274	89.957
$\langle \text{TL}_{\text{ext}} \rangle$	25.3	5.743	53.241	3.7	7.273	89.350
Lit. ⁶	25	6.129	37.794	3.3	7.790	61.392

For calculating the tunneling splittings based on the instanton approach it was found that an evidence-based approach starting from MEP and IP on the LL PES, augmented with geometries drawn from a pool of structures selected such that their RMSD is maximal with respect to an existing set of structures requires of the order of 50 points at the HL for TL. Therefore, only *local* and not global knowledge of the PES is required as would, e.g. be necessary for fully quantum-mechanical methods such as wavepackets. The bottleneck to a “direct” *ab initio*-based instanton approach is typically the calculation of N Hessians, as these are rather expensive to compute.^{11,12} Earlier work on instanton rate theory combined with machine-learning techniques for the $\text{H} + \text{CH}_4$ and $\text{H} + \text{C}_2\text{H}_6$ reactions required ~ 50 energies and forces and 8 Hessians in the training set to converge the rate constant to within 1 % of the *ab initio* result at 200 K.¹³ Using TL, calculating any high-level *ab initio* Hessians at all has been avoided. As is demonstrated here, this can significantly lower the computational expense with no loss of accuracy.

Table 5: Averaged harmonic frequencies calculated from PhysNet potentials and using *ab initio* techniques are given in cm^{-1} . As judged from the $\text{MAE}(\omega)$ the PhysNet model trained on the Extended Data Set containing 862 geometries is the most accurate, followed by the TL_2 (100 data points), TL_1 (50 data points) TL_{EB1} (25 data points) and TL_0 (25 data points). The *ab initio* harmonic frequencies obtained at the MP2 level are shown for comparison.

Mode	MP2	$\langle \text{TL}_0 \rangle$	$\langle \text{TL}_1 \rangle$	$\langle \text{TL}_2 \rangle$	$\langle \text{TL}_{\text{EB1}} \rangle$	$\langle \text{TL}_{\text{ext}} \rangle$	CCSD(T)
1	277.49	266.68	265.48	265.28	266.93	265.17	264.71
2	286.59	285.58	283.96	280.88	286.01	283.77	281.85
3	394.33	389.41	387.06	389.09	392.05	389.70	389.12
4	514.07	501.82	502.93	503.23	505.62	505.50	505.07
5	789.38	772.93	774.86	775.82	773.14	775.33	775.06
6	888.62	885.17	886.17	886.92	885.18	886.39	886.07
7	937.61	906.84	907.54	908.64	908.10	908.03	907.18
8	1012.29	988.09	989.05	992.64	991.79	990.78	989.73
9	1023.82	1005.95	1004.01	1002.71	1006.17	1002.93	1002.60
10	1048.75	1039.62	1039.69	1038.19	1039.50	1037.56	1037.85
11	1109.69	1104.46	1104.81	1102.64	1102.08	1102.20	1101.03
12	1288.28	1274.86	1271.94	1272.65	1272.27	1273.41	1272.73
13	1403.09	1400.18	1399.97	1401.56	1402.15	1401.73	1400.73
14	1407.97	1404.80	1408.40	1407.17	1406.59	1408.81	1406.94
15	1482.06	1458.89	1463.84	1463.95	1462.21	1467.70	1469.33
16	1641.52	1624.37	1627.95	1630.14	1631.91	1633.35	1632.52
17	1692.91	1681.91	1687.06	1691.27	1686.72	1693.59	1693.63
18	3039.02	3003.37	2999.68	2999.67	3005.82	3000.03	3001.26
19	3107.12	3176.46	3178.76	3180.11	3176.23	3176.74	3176.35
20	3217.85	3229.25	3228.54	3228.74	3232.47	3226.75	3227.12
21	3267.30	3259.40	3260.39	3262.98	3254.33	3263.25	3260.27
MAE	14.62	3.01	1.93	1.54	2.61	0.89	

With regards to the accuracy of the TL PESs it is of interest to compare their performance on out-of-sample structures. For this a test set was generated from MD simulations at 700 K on one of the TL_{ext} PESs from which 100 geometries were randomly extracted. In addition, 10 equally spaced off-grid geometries along the IP on the same PES were selected. The CCSD(T)/aug-cc-pVTZ energies of these 110 geometries cover a range from ~ 5 to 40 kcal/mol above the global minimum. The energies for these structures were computed based on TL_{ext} (most rigorous TL using 862 HL structures) and TL_{EB1} (following the recommended procedure; TL with 25 HL energies and forces), respectively, and the $[\text{MAE}_{100}(E), \text{MAE}_{10}(E)]$ for the two out-of-sample sets are [0.21,0.004] kcal/mol and [0.34,0.005] kcal/mol. Notably, the energies of the geometries used for TL_{ext} and TL_{EB1} only cover a range 20 kcal/mol above the global minimum whereas the out-of-sample energies reach twice as high, up to 40 kcal/mol above the minimum. Hence, the out-of-sample structures contain true predictions on the HL-PES. As a comparison, for the PIP PES, which used energies only and no forces, the reported fitting errors (i.e. in-sample) are 32 cm^{-1} (0.09 kcal/mol) for energies below 2000 cm^{-1} (5.7 kcal/mol) above the global minimum and 211 cm^{-1} (0.6 kcal/mol) for energies up to 20000 cm^{-1} (51.2 kcal/mol).²⁹

TL as used in the present work - namely as a local refinement of a LL-PES - can also be regarded as a variant of the more global “morphing” approach for PESs.⁵² It is therefore of interest to consider in what way observables other than the tunneling splitting change upon TL from LL to HL. For this, harmonic frequencies were determined for a number of transfer learned PESs. The harmonic frequencies averaged over the 10 individually trained NNs for different TLs are reported in Table 5, where they are compared with frequencies determined from CCSD(T)/aug-cc-pVTZ calculations at the corresponding equilibrium structure of malonaldehyde. As judged from the $\text{MAE}(\omega)$ the PhysNet model for TL_{ext} is most accurate ($\text{MAE} < 1 \text{ cm}^{-1}$), followed by TL_2 ($\text{MAE} < 2 \text{ cm}^{-1}$), TL_1 ($\text{MAE} \sim 2 \text{ cm}^{-1}$) and

TL₀ (MAE $\sim 3 \text{ cm}^{-1}$), as expected, and show a considerable improvement over the MP2 frequencies. For TL_{EB1} the MAE is $< 3 \text{ cm}^{-1}$. Thus, TL to the HL model also improves the shape of the PES in degrees orthogonal to the two reaction coordinates considered for the tunneling splitting.

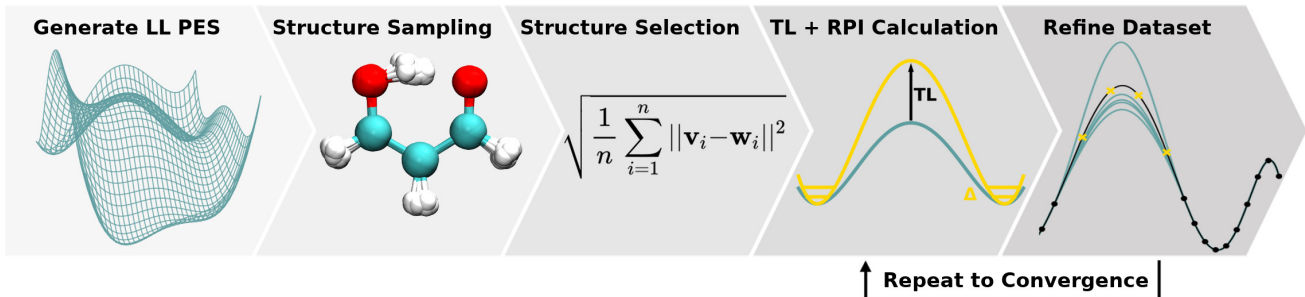


Figure 6: Flowchart of the recommended TL + RPI procedure.

In terms of a recommended procedure it is noted that the strategy outlined in going from TL₁ to TL₂ (adaptive sampling/active learning) can also be pursued recursively from a “pool” of geometries generated from sampling the PhysNet MP2 PES. This procedure can be repeated until convergence of the barrier height and the tunneling splittings. The approach proposed for future application is (see Figure 6): i) create a LL-PES from a fine grid (here 7×10^4 points) and train a ML model (here PhysNet) ii) generate a pool of structures based on the LL-PES (including MEP, Instanton, NMS) iii) choose $N \sim 25$ geometries following EB1/2 and determine energies and forces from HL *ab initio* calculations iv) perform TL and instanton calculations on the HL-PES v) refine the data set using adaptive sampling and structures along the *new* IP. Then repeat TL and instanton calculations vi) repeat iv) and v) until convergence. The present work demonstrates that following such a road-map requires ~ 50 HL energy and force evaluations to determine an accurate tunneling splitting of malonaldehyde which is manifestly more efficient than previously explored approaches.

In summary, given that LL models can be constructed efficiently even for moderately sized

molecules such as malonaldehyde or larger,⁵³ the present work confirms that with specific, evidence-based information grounded in physical understanding of the process in question, several 10 points from a HL treatment are sufficient to generate high-quality PESs for a target observable which was the tunneling splitting in malonaldehyde in the present work. The MAE(E) for the TL-PESs trained on energies spanning 20 kcal/mol above the global minimum is ~ 0.3 kcal/mol on off-grid structures spanning 40 kcal/mol and the resulting harmonic frequencies agree to within 1 to 3 cm^{-1} with rigorous and very time consuming normal mode analysis at the CCSD(T)/aug-cc-pVTZ level of theory. The recommended approach deduced from the present work is based on information about the MEP, the IP, and fluctuations around the IP determined on the LL-PES for which HL calculations are required for TL to determine the HL-PES. It is expected that - with suitable adaptations due to the particular observable considered - the present approach can also be applied to other observables that are computationally expensive to determine for a given PES, e.g. the quantum bound states of molecules or scattering cross sections for gas phase reactions from wavepacket propagation.

Acknowledgment

This work has been financially supported by the Swiss National Science Foundation NCCR-MUST (MM and JOR), the AFOSR, and the University of Basel.

References

- (1) Richardson, J. O.; Althorpe, S. C. Ring-polymer instanton method for calculating tunneling splittings. *J. Chem. Phys.* **2011**, *134*, 054109.

- (2) Richardson, J. O. Ring-polymer instanton theory. *Int. Rev. Phys. Chem.* **2018**, *37*, 171–216.
- (3) Richardson, J. O.; Pérez, C.; Lobsiger, S.; Reid, A. A.; Temelso, B.; Shields, G. C.; Kisiel, Z.; Wales, D. J.; Pate, B. H.; Althorpe, S. C. Concerted Hydrogen-Bond Breaking by Quantum Tunneling in the Water Hexamer Prism. *Science* **2016**, *351*, 1310–1313.
- (4) Richardson, J. O. Full-and reduced-dimensionality instanton calculations of the tunnelling splitting in the formic acid dimer. *Phys. Chem. Chem. Phys.* **2017**, *19*, 966–970.
- (5) Coleman, S. The uses of instantons. 1977; Also in S. Coleman, *Aspects of Symmetry*, chapter 7, pp. 265–350 (Cambridge University Press, 1985).
- (6) Jahr, E.; Laude, G.; Richardson, J. O. Instanton theory of tunneling in molecules with asymmetric isotopic substitutions. *J. Chem. Phys.* **2020**, *153*, 094101.
- (7) Hammer, T.; Manthe, U. Intramolecular proton transfer in malonaldehyde: Accurate multilayer multi-configurational time-dependent Hartree calculations. *J. Chem. Phys.* **2011**, *134*, 224305.
- (8) Schröder, M.; Gatti, F.; Meyer, H.-D. Theoretical studies of the tunneling splitting of malonaldehyde using the multiconfiguration time-dependent Hartree approach. *J. Chem. Phys.* **2011**, *134*, 234307.
- (9) Mátyus, E.; Wales, D. J.; Althorpe, S. C. Quantum tunneling splittings from path-integral molecular dynamics. *J. Chem. Phys.* **2016**, *144*, 114108.
- (10) Vaillant, C. L.; Wales, D. J.; Althorpe, S. C. Tunneling splittings from path-integral molecular dynamics using a Langevin thermostat. *J. Chem. Phys.* **2018**, *148*, 234102.
- (11) Mil'nikov, G. V.; Yagi, K.; Taketsugu, T.; Nakamura, H.; Hirao, K. Tunneling splitting in polyatomic molecules: Application to malonaldehyde. *J. Chem. Phys.* **2003**, *119*, 10–13.

- (12) Sahu, N.; Richardson, J. O.; Berger, R. Instanton calculations of tunneling splittings in chiral molecules. *J. Comput. Chem.* **2021**, *42*, 210–221.
- (13) Laude, G.; Calderini, D.; Tew, D. P.; Richardson, J. O. Ab initio instanton rate theory made efficient using Gaussian process regression. *Faraday Discuss.* **2018**, *212*, 237–258.
- (14) Cooper, A. M.; Hallmen, P. P.; Kästner, J. Potential energy surface interpolation with neural networks for instanton rate calculations. *J. Chem. Phys.* **2018**, *148*, 094106.
- (15) McConnell, S. R.; Kästner, J. Instanton rate constant calculations using interpolated potential energy surfaces in nonredundant, rotationally and translationally invariant coordinates. *J. Comput. Chem.* **2019**, *40*, 866–874.
- (16) Unke, O. T.; Koner, D.; Patra, S.; Käser, S.; Meuwly, M. High-dimensional potential energy surfaces for molecular simulations: from empiricism to machine learning. *Mach. learn.: sci. technol.* **2020**, *1*, 013001.
- (17) Friesner, R. A. Ab initio quantum chemistry: Methodology and applications. *Proc. Natl. Acad. Sci. USA* **2005**, *102*, 6648–6653.
- (18) Pan, S. J.; Yang, Q. A survey on transfer learning. *IEEE Trans. Knowl. Data Eng.* **2009**, *22*, 1345–1359.
- (19) Taylor, M. E.; Stone, P. Transfer learning for reinforcement learning domains: A survey. *J. Mach. Learn. Res.* **2009**, *10*, 1633–1685.
- (20) Smith, J. S.; Nebgen, B. T.; Zubatyuk, R.; Lubbers, N.; Devereux, C.; Barros, K.; Tretiak, S.; Isayev, O.; Roitberg, A. E. Approaching coupled cluster accuracy with a general-purpose neural network potential through transfer learning. *Nat. Commun.* **2019**, *10*, 1–8.

- (21) Ramakrishnan, R.; Dral, P.; Rupp, M.; von Lilienfeld, O. A. Big Data meets quantum chemistry approximations: The Δ -machine learning approach. *J. Chem. Theory Comput.* **2015**, *11*, 2087–2096.
- (22) Käser, S.; Unke, O. T.; Meuwly, M. Reactive dynamics and spectroscopy of hydrogen transfer from neural network-based reactive potential energy surfaces. *New J. Phys.* **2020**, *22*, 055002.
- (23) Käser, S.; Koner, D.; Christensen, A. S.; von Lilienfeld, O. A.; Meuwly, M. Machine Learning Models of Vibrating H₂CO: Comparing Reproducing Kernels, FCHL, and PhysNet. *J. Phys. Chem. A* **2020**, *124*, 8853–8865.
- (24) Nandi, A.; Qu, C.; Houston, P. L.; Conte, R.; Bowman, J. M. Δ -machine learning for potential energy surfaces: A PIP approach to bring a DFT-based PES to CCSD(T) level of theory. *J. Chem. Phys.* **2021**, *154*, 051102.
- (25) Käser, S.; Boittier, E. D.; Upadhyay, M.; Meuwly, M. Transfer Learning to CCSD(T): Accurate Anharmonic Frequencies from Machine Learning Models. *J. Chem. Theory Comput.* **2021**, *17*, 3687–3699.
- (26) Qu, C.; Houston, P. L.; Conte, R.; Nandi, A.; Bowman, J. M. Breaking the Coupled Cluster Barrier for Machine-Learned Potentials of Large Molecules: The Case of 15-Atom Acetylacetone. *J. Phys. Chem. Lett.* **2021**, *12*, 4902–4909.
- (27) Käser, S.; Meuwly, M. Transfer learned potential energy surfaces: accurate anharmonic vibrational dynamics and dissociation energies for the formic acid monomer and dimer. *Phys. Chem. Chem. Phys.* **2022**, *24*, 5269–5281.
- (28) Laude, G.; Calderini, D.; Welsch, R.; Richardson, J. O. Calculations of quantum tunnelling rates for Muonium reactions with methane, ethane and propane. *Phys. Chem. Chem. Phys.* **2020**, *22*, 16843–16854.

- (29) Wang, Y.; Braams, B. J.; Bowman, J. M.; Carter, S.; Tew, D. P. Full-dimensional quantum calculations of ground-state tunneling splitting of malonaldehyde using an accurate ab initio potential energy surface. *J. Chem. Phys.* **2008**, *128*, 224314.
- (30) Cvitas, M. T.; Althorpe, S. C. Locating instantons in calculations of tunneling splittings: The test case of malonaldehyde. *J. Chem. Theory Comput.* **2016**, *12*, 787–803.
- (31) Mizukami, W.; Habershon, S.; Tew, D. P. A compact and accurate semi-global potential energy surface for malonaldehyde from constrained least squares regression. *J. Chem. Phys.* **2014**, *141*, 144310.
- (32) Firth, D.; Beyer, K.; Dvorak, M.; Reeve, S.; Grushow, A.; Leopold, K. Tunable far-infrared spectroscopy of malonaldehyde. *J. Chem. Phys.* **1991**, *94*, 1812–1819.
- (33) Baba, T.; Tanaka, T.; Morino, I.; Yamada, K. M.; Tanaka, K. Detection of the tunneling-rotation transitions of malonaldehyde in the submillimeter-wave region. *J. Chem. Phys.* **1999**, *110*, 4131–4133.
- (34) Redington, R. L.; Redington, T. E.; Sams, R. L. Infrared Absorption Spectra in the Hydroxyl Stretching Regions of Gaseous Tropolone OHO Isotopomers. *Z. Phys. Chem.* **2008**, *222*, 1197–1211.
- (35) Murdock, D.; Burns, L. A.; Vaccaro, P. H. Vibrational specificity of proton-transfer dynamics in ground-state tropolone. *Phys. Chem. Chem. Phys.* **2010**, *12*, 8285–8299.
- (36) Ortlieb, M.; Havenith, M. Proton transfer in (HCOOH)₂: an IR high-resolution spectroscopic study of the antisymmetric C–O stretch. *J. Phys. Chem. A* **2007**, *111*, 7355–7363.
- (37) Zhang, Y.; Li, W.; Luo, W.; Zhu, Y.; Duan, C. High resolution jet-cooled infrared absorption spectra of (HCOOH)₂, (HCOOD)₂, and HCOOH-HCOOD complexes in 7.2 μm region. *J. Chem. Phys.* **2017**, *146*, 244306.

- (38) Li, W.; Evangelisti, L.; Gou, Q.; Caminati, W.; Meyer, R. The barrier to proton transfer in the dimer of formic acid: a pure rotational study. *Angew. Chem. Int. Ed. Engl.* **2019**, *58*, 859–865.
- (39) Insausti, A.; Ma, J.; Yang, Q.; Xie, F.; Xu, Y. Rotational Spectroscopy of 2-Furoic Acid and Its Dimer: Conformational Distribution and Double Proton Tunneling. *ChemPhysChem* **2022**, *23*, e202200176.
- (40) Baughcum, S. L.; Smith, Z.; Wilson, E. B.; Duerst, R. W. Microwave spectroscopic study of malonaldehyde. 3. Vibration-rotation interaction and one-dimensional model for proton tunneling. *J. Am. Chem. Soc.* **1984**, *106*, 2260–2265.
- (41) Mil’nikov, G. V.; Nakamura, H. Practical implementation of the instanton theory for the ground-state tunneling splitting. *J. Chem. Phys.* **2001**, *115*, 6881–6897.
- (42) Richardson, J. O. Perspective: Ring-polymer instanton theory. *J. Chem. Phys.* **2018**, *148*, 200901.
- (43) Richardson, J. O.; Althorpe, S. C.; Wales, D. J. Instanton calculations of tunneling splittings for water dimer and trimer. *J. Chem. Phys.* **2011**, *135*, 124109.
- (44) Unke, O. T.; Meuwly, M. PhysNet: A neural network for predicting energies, forces, dipole moments, and partial charges. *J. Chem. Theory Comput.* **2019**, *15*, 3678–3693.
- (45) Gilmer, J.; Schoenholz, S. S.; Riley, P. F.; Vinyals, O.; Dahl, G. E. Neural message passing for quantum chemistry. Proc. of the 34th Int. Conf. on Machine Learning-Volume 70. 2017; pp 1263–1272.
- (46) Baydin, A. G.; Pearlmutter, B. A.; Radul, A. A.; Siskind, J. M. Automatic differentiation in machine learning: a survey. *J. Mach. Learn. Res.* **2017**, *18*, 5595–5637.
- (47) Abadi, M.; Barham, P.; Chen, J.; Chen, Z.; Davis, A.; Dean, J.; Devin, M.; Ghemawat, S.; Irving, G.; Isard, M. et al. Tensorflow: A system for large-scale machine

- learning. 12th USENIX symposium on operating systems Design and Implementation (OSDI 16). 2016; pp 265–283.
- (48) Werner, H.-J.; Knowles, P. J.; Knizia, G.; Manby, F. R.; Schütz, M.; Celani, P.; Györfy, W.; Kats, D.; Korona, T.; Lindh, R. et al. MOLPRO, version 2019, a package of ab initio programs. 2019.
- (49) Behler, J. Constructing high-dimensional neural network potentials: A tutorial review. *Int. J. Quantum. Chem.* **2015**, *115*, 1032–1050.
- (50) Meisner, J.; Kästner, J. Dual-Level Approach to Instanton Theory. *J. Chem. Theory Comput.* **2018**, *14*, 1865–1872.
- (51) Heller, E. R.; Richardson, J. O. Heavy-Atom Quantum Tunnelling in Spin Crossovers of Nitrenes. *Angew. Chem. Int. Ed.* **2022**,
- (52) Meuwly, M.; Hutson, J. Morphing Ab Initio Potentials: A Systematic Study of Ne-HF. *J. Chem. Phys.* **1999**, *110*, 8338–8347.
- (53) Koner, D.; Meuwly, M. Permutationally invariant, reproducing kernel-based potential energy surfaces for polyatomic molecules: From formaldehyde to acetone. *J. Chem. Theory Comput.* **2020**, *16*, 5474–5484.

Supporting Information: Transfer learning for affordable and high quality tunneling splittings from instanton calculations

Silvan Käser,[†] Jeremy O. Richardson,[‡] and Markus Meuwly^{*,†}

[†]*Department of Chemistry, University of Basel, Klingelbergstrasse 80 , CH-4056 Basel,
Switzerland.*

[‡]*Laboratory of Physical Chemistry, ETH Zurich, 8093 Zurich, Switzerland.*

E-mail: m.meuwly@unibas.ch

August 3, 2022

Table S1: Tunneling splittings in cm^{-1} for MA determined from the PhysNet MP2 PES.¹ Convergence is tested by looking down the diagonals of the table from which the optimal working effective temperature and N can be determined.² Here 25 K and $N \geq 1024$ is seen to be sufficient.

$N \setminus T$	50 K	25 K	12.5 K
512	96	94	87
1024	97	96	94
2048	97	96	96
4096	97	96	96

Table S2: Energy barriers E_B (kcal/mol), tunneling splittings Δ (in cm^{-1}) at $T = 25$ K and with $N = 4096$, action S/\hbar and fluctuation factor Φ for deuterated MA determined from TL_{ext} and $\text{TL}_{0,1,2}$ PESs. The *ab initio* barrier height for HT at the CCSD(T)/aug-cc-pVTZ level of theory is 3.8948 kcal/mol.

	N_{data}	E_B	Δ_D	S/\hbar	Φ
MP2	70k	2.7889	18.8	5.705	73.964
$\langle \text{TL}_0 \rangle$	25	3.8925 ± 0.0119	3.3 ± 0.3	7.281 ± 0.030	97.876 ± 7.794
$\langle \text{TL}_1 \rangle$	50	3.8974 ± 0.0161	3.5 ± 0.2	7.297 ± 0.014	90.997 ± 4.188
$\langle \text{TL}_2 \rangle$	100	3.8941 ± 0.0021	3.6 ± 0.1	7.279 ± 0.006	89.754 ± 2.126
$\langle \text{TL}_{\text{ext}} \rangle$	862	3.8945 ± 0.0006	3.7 ± 0.0	7.273 ± 0.002	89.350 ± 0.762

Table S3: Energy barriers E_B (kcal/mol), tunneling splittings Δ_0 (at $T = 25$ K and $N = 4096$ given in cm^{-1}), action S/\hbar and fluctuation factor Φ for MA and deuterated MA determined from TL_{ext} PES using an extended data set.

$\text{TL}_{\text{ext}}^{\#}$	E_B	H			D		
		Δ_0	S/\hbar	Φ	Δ_0	S/\hbar	Φ
0	3.8938	25.1	5.744	53.586	3.64	7.273	89.957
1	3.8942	25.4	5.742	52.925	3.70	7.272	88.696
2	3.8942	25.6	5.744	52.513	3.71	7.274	88.308
3	3.8938	24.9	5.740	54.138	3.61	7.270	91.017
4	3.8939	25.3	5.740	53.238	3.69	7.270	89.014
5	3.8953	25.1	5.745	53.418	3.65	7.275	89.498
6	3.8943	25.4	5.743	52.959	3.69	7.273	88.870
7	3.8953	25.4	5.743	52.943	3.67	7.273	89.321
8	3.8953	25.1	5.744	53.542	3.65	7.275	89.723
9	3.8950	25.4	5.741	53.142	3.69	7.271	89.097
$\langle \text{TL}_{\text{ext}} \rangle$	3.8945	25.3	5.743	53.241	3.67	7.273	89.350
σ	0.0006	0.2	0.002	0.454	0.03	0.002	0.762

Table S4: Energy barriers E_B (kcal/mol), tunneling splittings Δ_0 (at $T = 25$ K and $N = 4096$ given in cm^{-1}), action S/\hbar and fluctuation factor Φ for MA and deuterated MA determined from TL_0 PES using a data set containing 50 structures.

$\text{TL}_0^{\#}$	E_B	H			D		
		Δ_0	S/\hbar	Φ	Δ_0	S/\hbar	Φ
0	3.8877	21.5	5.760	61.639	3.04	7.292	105.980
1	3.8935	26.6	5.696	52.768	3.88	7.225	88.422
2	3.8841	22.2	5.745	60.600	3.18	7.276	102.895
3	3.8976	24.6	5.749	54.460	3.49	7.284	93.066
4	3.8844	21.4	5.745	62.833	3.05	7.274	107.429
5	3.8926	25.1	5.781	51.690	3.50	7.318	89.771
6	3.8904	25.4	5.736	53.338	3.65	7.266	90.392
7	3.8771	22.2	5.734	61.140	3.18	7.264	103.839
8	3.9214	23.8	5.793	53.925	3.37	7.336	91.624
9	3.8958	21.8	5.745	61.659	3.10	7.277	105.346
$\langle \text{TL}_0 \rangle$	3.8925	23.4	5.749	57.405	3.34	7.281	97.876
σ	0.0119	1.9	0.026	4.486	0.28	0.030	7.794

Table S5: Energy barriers E_B (kcal/mol), tunneling splittings Δ_0 (at $T = 25$ K and $N = 4096$ given in cm^{-1}), action S/\hbar and fluctuation factor Φ for MA and deuterated MA determined from TL_1 PES using a data set containing 50 structures.

$\text{TL}_1^\#$	E_B	H			D		
		Δ_0	S/\hbar	Φ	Δ_0	S/\hbar	Φ
0	3.8526	26.3	5.783	49.262	3.75	7.319	83.824
1	3.9004	24.4	5.759	54.272	3.46	7.291	93.226
2	3.9002	25.5	5.750	52.310	3.61	7.283	90.000
3	3.9056	24.1	5.768	54.546	3.38	7.301	94.446
4	3.9029	27.1	5.748	49.444	3.84	7.279	84.932
5	3.9019	24.2	5.766	54.405	3.45	7.299	92.843
6	3.9099	25.0	5.783	51.920	3.54	7.320	88.713
7	3.8972	23.4	5.756	56.820	3.33	7.288	97.192
8	3.9022	24.4	5.769	53.811	3.48	7.302	91.769
9	3.9014	24.5	5.757	54.174	3.47	7.288	93.026
$\langle \text{TL}_1 \rangle$	3.8974	24.9	5.764	53.096	3.53	7.297	90.997
σ	0.0161	1.1	0.012	2.375	0.16	0.014	4.188

Table S6: Energy barriers E_B (kcal/mol), tunneling splittings Δ_0 (at $T = 25$ K and $N = 4096$ given in cm^{-1}), action S/\hbar and fluctuation factor Φ for MA and deuterated MA determined from TL_2 PES using a data set containing 100 structures.

$\text{TL}_2^\#$	E_B	H			D		
		Δ_0	S/\hbar	Φ	Δ_0	S/\hbar	Φ
0	3.8950	25.1	5.754	53.109	3.60	7.285	90.133
1	3.8974	24.8	5.753	53.760	3.55	7.285	91.390
2	3.8931	24.8	5.742	54.284	3.62	7.272	90.596
3	3.8920	25.9	5.751	51.488	3.72	7.282	87.312
4	3.8922	26.0	5.744	51.648	3.74	7.273	87.720
5	3.8932	25.5	5.746	52.648	3.68	7.276	88.701
6	3.8942	24.8	5.753	53.636	3.55	7.285	91.271
7	3.8968	25.5	5.752	52.316	3.67	7.283	88.488
8	3.8959	25.6	5.743	52.528	3.73	7.272	87.869
9	3.8917	24.4	5.745	55.116	3.48	7.274	94.056
$\langle \text{TL}_2 \rangle$	3.8941	25.2	5.748	53.053	3.63	7.279	89.754
σ	0.0021	0.5	0.005	1.156	0.09	0.006	2.126

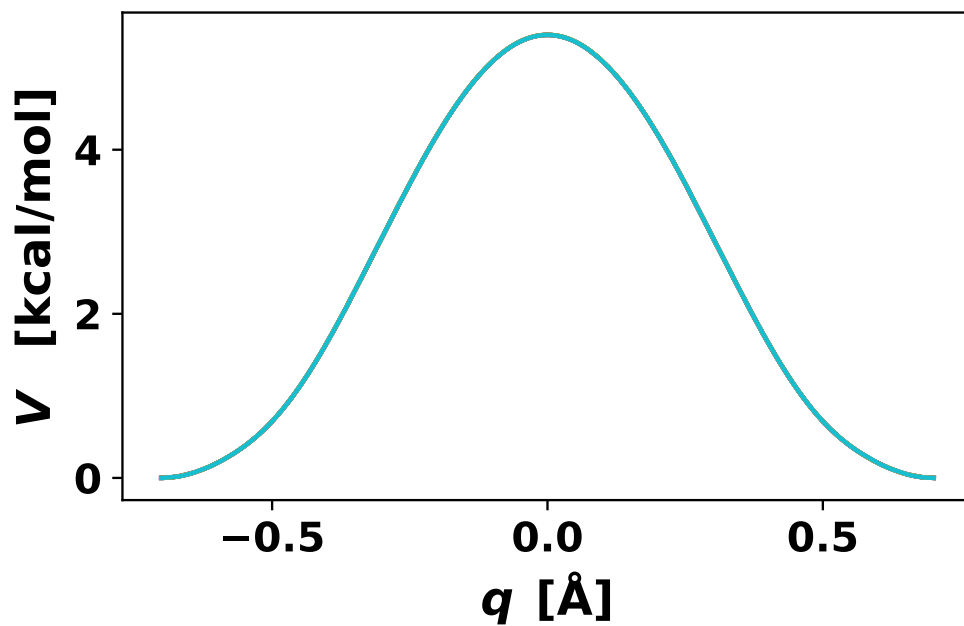


Figure S1: Overlay of the instanton path obtained from the ten TLs using the extended data set, TL_{ext} . q corresponds to $q = r_{\text{OAH}} - r_{\text{OBH}}$.

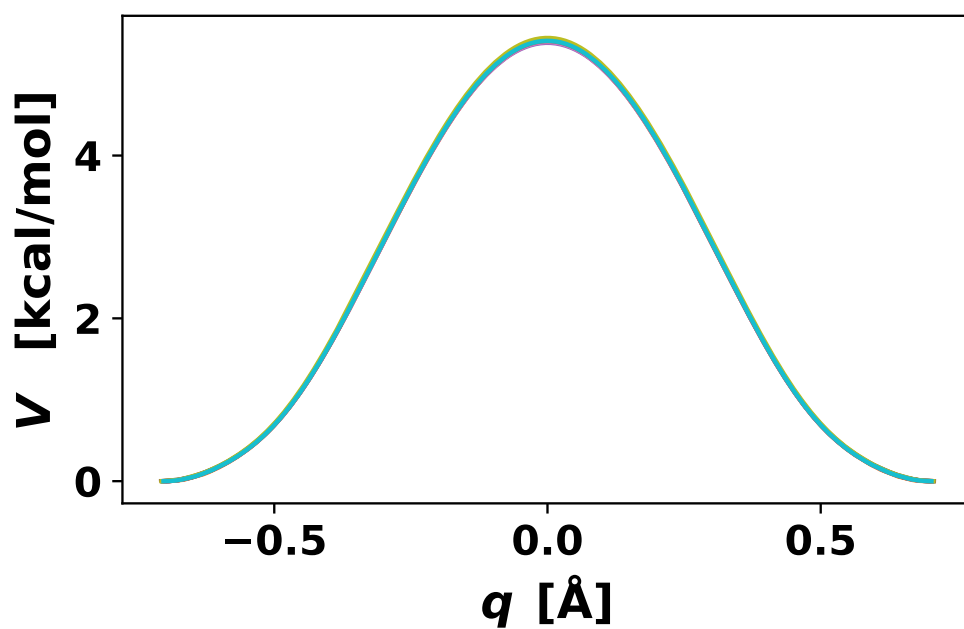


Figure S2: Overlay of the instanton path obtained from the ten TLs from TL_0 . q corresponds to $q = r_{\text{OAH}} - r_{\text{OBH}}$.

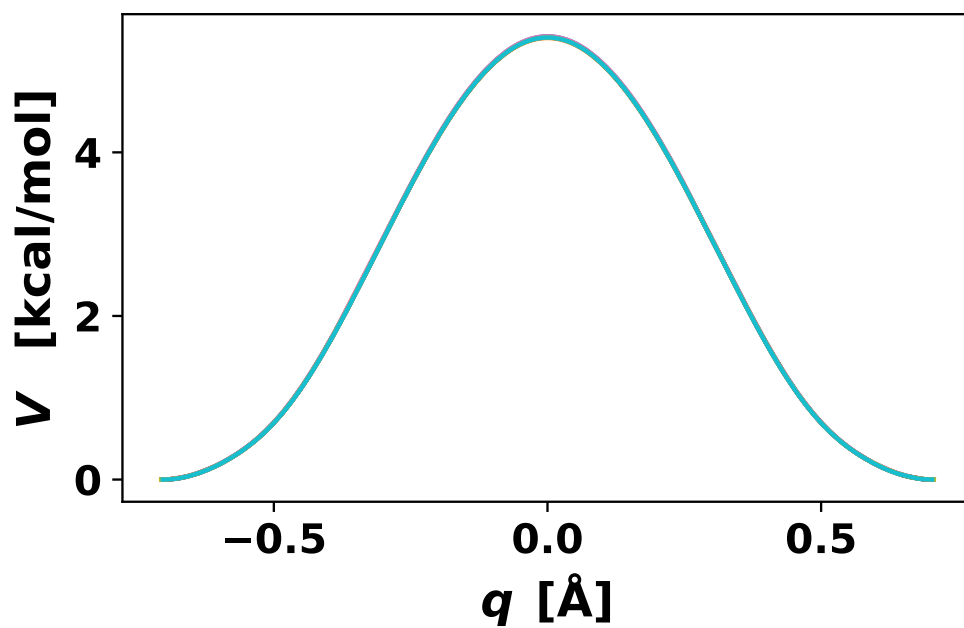


Figure S3: Overlay of the instanton path obtained from the ten TLs from TL_1 . q corresponds to $q = r_{O_{AH}} - r_{O_{BH}}$.

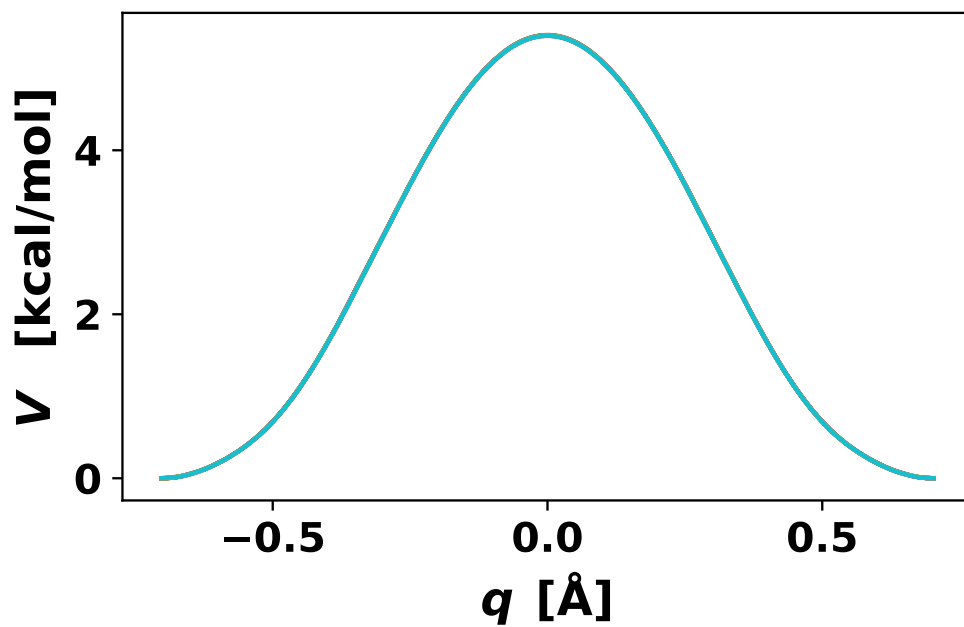


Figure S4: Overlay of the instanton path obtained from the ten TLs from TL_2 . q corresponds to $q = r_{O_{AH}} - r_{O_{BH}}$.

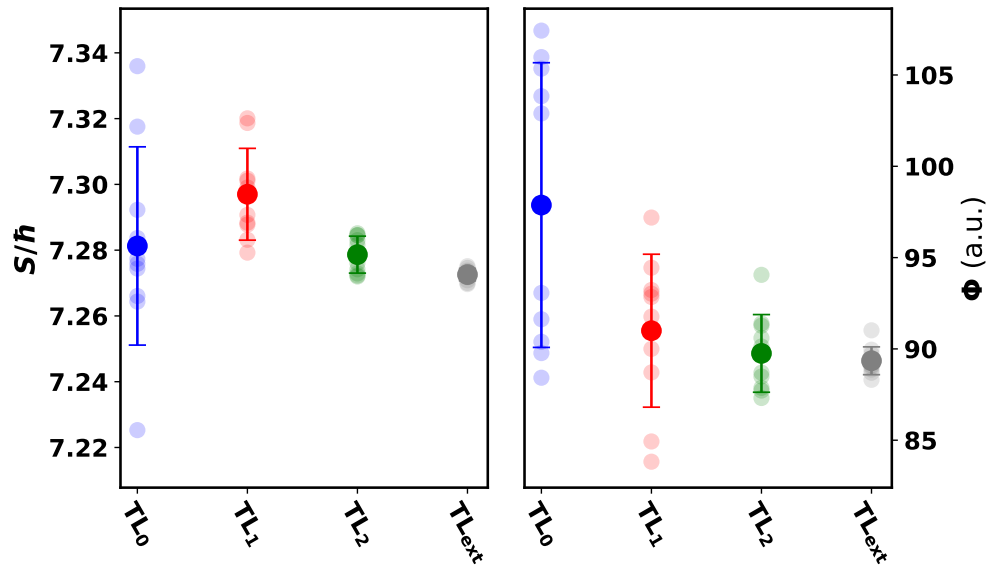


Figure S5: Action S/\hbar and fluctuation factor Φ from all TL PESs (transparent circles), the corresponding averages (opaque circle) and standard deviations (error bars as $\pm\sigma$) as obtained from TL_0 (blue), TL_1 (red), TL_2 (green) and TL_{ext} for DT.

Table S7: Summary of recent work on ground state tunneling splitting for MA. E_B is given in kcal/mol. The results emphasized in red are supposed to be closest to the present results due to a similar PES and method to obtain the tunneling splittings (RPI).

	Ref.	PES	E_B	Dynamics	H/D	Δ [cm^{-1}]	
Exp.	3,4				H	21.583	
	5				D	2.915	
Theo.	6	FF ^a	10.0	semiclassical ^b	H	21.8	
	7	FF ^{a,g}	10.0	RPI ⁱ	H	51	
	8	AI ^c (B3LYP/double- ζ)	2.3	semiclassical ^b	H	21 ± 1	
	9	SI ^d (MP2/6-31G(d,p)) ¹⁰	3.6	instanton	H	30.7	
	11	SI (MP2/6-31G(d,p)) ¹⁰	3.6	POITSE ^e	H	25.7 ± 0.3	
	12	AI (MC-QCISD/3)	4.1	rainbow instanton	H	25.4	
	9	AI (CCSD(T)/(a)VTZ)	3.8	instanton	H	21 - 22	
	13	PIP ^f (CCSD(T)/aVTZ)	4.1	DMC	H	$21.6 \pm (2 - 3)$	
	14	PIP (CCSD(T)/aVTZ)	4.1	MCTDH ^g	H	23.4	
	15	PIP (CCSD(T)/aVTZ)	4.1	MCTDH	H	23.8	
	16	PIP (CCSD(T)/aVTZ)	4.1	RPI	H	25	
	17	PIP (CCSD(T)/aVTZ)	4.1	RPI	H	24.9	
	18	PIP (CCSD(T)/aVTZ)	4.1	ti-QM ^h	H	24.5	
	17	LASSO ^j (CCSD(T)(F12*))	4.0	RPI	H	19.3	
		9	SI (MP2/6-31G(d,p)) ¹⁰	3.6	instanton	D	4.58
		11	SI (MP2/6-31G(d,p)) ¹⁰	3.6	POITSE	D	3.21 ± 0.09
		12	AI (MC-QCISD/3)	4.1	rainbow instanton	D	3.4
		9	AI (CCSD(T)/(a)VTZ)	3.8	instanton	D	3.0
		13	PIP (CCSD(T)/aVTZ)	4.1	DMC	D	$3.0 \pm (2 - 3)$
		16	PIP (CCSD(T)/aVTZ)	4.1	RPI	D	3.4

^a experimental vibrational force field derived by Wilson et al.^{19,20}

^b semiclassical method based on the Makri-Miller model

^c *Ab initio*

^d Shepard interpolation

^e Monte Carlo projection operator, imaginary time spectral evolution

^f Permutationally invariant polynomial method

^g Multiconfiguration time-dependent Hartree approach

^h time-independent quantum mechanical method

ⁱ Ring-polymer instanton method

^j least absolute shrinkage and selection operator

References

- (1) Käser, S.; Unke, O. T.; Meuwly, M. Reactive dynamics and spectroscopy of hydrogen transfer from neural network-based reactive potential energy surfaces. *New J. Phys.* **2020**, *22*, 055002.
- (2) Richardson, J. O.; Althorpe, S. C. Ring-polymer instanton method for calculating tunneling splittings. *J. Chem. Phys.* **2011**, *134*, 054109.
- (3) Firth, D.; Beyer, K.; Dvorak, M.; Reeve, S.; Grushow, A.; Leopold, K. Tunable far-infrared spectroscopy of malonaldehyde. *J. Chem. Phys.* **1991**, *94*, 1812–1819.
- (4) Baba, T.; Tanaka, T.; Morino, I.; Yamada, K. M.; Tanaka, K. Detection of the tunneling-rotation transitions of malonaldehyde in the submillimeter-wave region. *J. Chem. Phys.* **1999**, *110*, 4131–4133.
- (5) Baughcum, S. L.; Smith, Z.; Wilson, E. B.; Duerst, R. W. Microwave spectroscopic study of malonaldehyde. 3. Vibration-rotation interaction and one-dimensional model for proton tunneling. *J. Am. Chem. Soc.* **1984**, *106*, 2260–2265.
- (6) Sewell, T. D.; Guo, Y.; Thompson, D. L. Semiclassical calculations of tunneling splitting in malonaldehyde. *J. Chem. Phys.* **1995**, *103*, 8557–8565.
- (7) Richardson, J. O.; Althorpe, S. C. Ring-polymer instanton method for calculating tunneling splittings. *J. Chem. Phys.* **2011**, *134*, 054109.
- (8) Ben-Nun, M.; Martínez, T. J. Semiclassical tunneling rates from ab initio molecular dynamics. *J. Phys. Chem. A* **1999**, *103*, 6055–6059.
- (9) Mil'nikov, G. V.; Yagi, K.; Taketsugu, T.; Nakamura, H.; Hirao, K. Simple and accurate method to evaluate tunneling splitting in polyatomic molecules. *J. Chem. Phys.* **2004**, *120*, 5036–5045.

- (10) Yagi, K.; Taketsugu, T.; Hirao, K. Generation of full-dimensional potential energy surface of intramolecular hydrogen atom transfer in malonaldehyde and tunneling dynamics. *J. Chem. Phys.* **2001**, *115*, 10647–10655.
- (11) Viel, A.; Coutinho-Neto, M. D.; Manthe, U. The ground state tunneling splitting and the zero point energy of malonaldehyde: A quantum Monte Carlo determination. *J. Chem. Phys.* **2007**, *126*, 024308.
- (12) Smedarchina, Z.; Siebrand, W.; Fernández-Ramos, A. The rainbow instanton method: A new approach to tunneling splitting in polyatomics. *J. Chem. Phys.* **2012**, *137*, 224105.
- (13) Wang, Y.; Braams, B. J.; Bowman, J. M.; Carter, S.; Tew, D. P. Full-dimensional quantum calculations of ground-state tunneling splitting of malonaldehyde using an accurate ab initio potential energy surface. *J. Chem. Phys.* **2008**, *128*, 224314.
- (14) Schröder, M.; Gatti, F.; Meyer, H.-D. Theoretical studies of the tunneling splitting of malonaldehyde using the multiconfiguration time-dependent Hartree approach. *J. Chem. Phys.* **2011**, *134*, 234307.
- (15) Hammer, T.; Manthe, U. Intramolecular proton transfer in malonaldehyde: Accurate multilayer multi-configurational time-dependent Hartree calculations. *J. Chem. Phys.* **2011**, *134*, 224305.
- (16) Cvitas, M. T.; Althorpe, S. C. Locating instantons in calculations of tunneling splittings: The test case of malonaldehyde. *J. Chem. Theory Comput.* **2016**, *12*, 787–803.
- (17) Jahr, E.; Laude, G.; Richardson, J. O. Instanton theory of tunneling in molecules with asymmetric isotopic substitutions. *J. Chem. Phys.* **2020**, *153*, 094101.
- (18) Wu, F.; Ren, Y.; Bian, W. The hydrogen tunneling splitting in malonaldehyde: A

- full-dimensional time-independent quantum mechanical method. *J. Chem. Phys.* **2016**, *145*, 074309.
- (19) Smith, Z.; Wilson, E. B.; Duerst, R. W. The infrared spectrum of gaseous malonaldehyde (3-hydroxy-2-propenal). *Spectrochim. Acta A Mol. Biomol. Spectrosc.* **1983**, *39*, 1117–1129.
- (20) Baughcum, S. L.; Duerst, R. W.; Rowe, W. F.; Smith, Z.; Wilson, E. B. Microwave spectroscopic study of malonaldehyde (3-hydroxy-2-propenal). 2. Structure, dipole moment, and tunneling. *J. Am. Chem. Soc.* **1981**, *103*, 6296–6303.